Article

Beach Monitoring and Morphological Response in the Presence of Coastal Defense Strategies at Riccione (Italy)

Claudia Romagnoli [1,*], Flavia Sistilli [1], Luigi Cantelli [1], Margherita Aguzzi [2], Nunzio De Nigris [2], Maurizio Morelli [2], Maria Gabriella Gaeta [3] and Renata Archetti [3]

1   Department of Biological, Geological and Environmental Sciences (BiGeA), University of Bologna, 40126 Bologna, Italy; flavia.sistilli2@unibo.it (F.S.); luigi.cantelli@unibo.it (L.C.)
2   Regional Agency for Prevention, Environment and Energy, Emilia-Romagna (Arpae), 40122 Bologna, Italy; maguzzi@arpae.it (M.A.); ndenigris@arpae.it (N.D.N.); mauriziomorelli@arpae.it (M.M.)
3   Department of Civil, Environmental, Chemical and Materials Engineering (DICAM), University of Bologna, 40136 Bologna, Italy; g.gaeta@unibo.it (M.G.G.); renata.archetti@unibo.it (R.A.)
*   Correspondence: claudia.romagnoli@unibo.it

Abstract: The coastal area at Riccione, in the southern Emilia-Romagna littoral region, is exposed to erosive processes, which are expected to be enhanced by climate change. The beach, mostly composed of fine sand, is maintained through various defense strategies, including frequent nourishment interventions for balancing the sediment deficit and other experimental solutions for reducing coastal erosion. Artificial reshaping of the beach and "common practices" in the sediment management redefine the beach morphology and the sediment redistribution almost continuously. These activities overlap each other and with the coastal dynamics, and this makes it very difficult to evaluate their effectiveness, as well as the role of natural processes on the beach morphological evolution. Topo-bathymetric and sedimentological monitoring of the beach has been carried out on a regular basis since 2000 by the Regional Agency for Prevention, Environment and Energy of Emilia-Romagna (Arpae). Further monitoring of the emerged and submerged beach has been carried out in 2019–2021 in the framework of the research project STIMARE, focusing on innovative strategies for coastal monitoring in relation with erosion risk. The aim of this study is to assess the coastal behavior at the interannual/seasonal scale in the southern coastal stretch of Riccione, where the adopted coastal defense strategies and management actions mostly control the morphological variations in the emerged and submerged beach besides the wave and current regime. The topo-bathymetric variations and erosion/accretion patterns provided by multitemporal monitoring have been related to natural processes and to anthropogenic activities. The morphological variations have been also assessed in volumetric terms in the different subzones of the beach, with the aim of better understanding the onshore/offshore sediment exchange in relation with nourishments and in the presence of protection structures. The effectiveness of the adopted interventions to combat erosion, and to cope with future climate change-related impacts, appears not fully successful in the presence of an overall sediment deficit at the coast. This demonstrates the need for repeated monitoring of the emerged and submerged beach in such a critical setting.

Keywords: topo-bathymetric surveys; beach morphological variations; coastal erosion; defense interventions; climate change impacts

1. Introduction

Coastal dynamics in the Emilia-Romagna region are widely controlled by anthropogenic factors. About ~50% of the coast is potentially subjected to erosion and is maintained in equilibrium conditions through various defense approaches [1]. The use of the coast for tourism markedly grew in the second half of the XX century, becoming one of the most important economic activities of the region. The urban settlement increased as well, and the coastal area has lost its natural setting. Moreover, a large part of the coast does not

exceed 2 m above sea level and part of the hinterland is currently below sea level. This may enhance the impacts of climate change, such as erosion and flooding due to extreme meteorological events and sea-level rise [2–4].

To evaluate the state and evolution of a coastal area, morphological changes and volumetric variations (not limited to the subaerial beach but also extending to the nearshore) are considered to be more significant indicators for assessing the overall sedimentary budget than the shoreline behavior, which is very variable and often affected by anthropic bias [5]. While a wide-ranging literature exists on the morphodynamics of natural beaches and their response to variations in the wave climate [6–8], fewer papers deal with the morphological response of beaches in the presence of coastal structures or after nourishment interventions [9–11], in contrast with the need for assessing the effectiveness of the adopted strategies in relation with the local coastal dynamics. Coastal monitoring is a fundamental tool for this purpose; it is necessary for supporting management and decision-making initiatives, especially in the view of climate changes and related impacts [12]. Monitoring can be carried out through different techniques and approaches, depending on several variables such as duration and areal extent, accuracy, spatio-temporal resolution and costs [13]. In any case, the integration of data on emerged and submerged beaches, despite not being frequently performed, is necessary for a correct understanding of the overall beach morphological evolution and of the cross-shore and longshore sediment movement at the coast. Recent remote sensing techniques for investigating the nearshore bathymetry include satellite [14–16] and Lidar applications [17,18] or both (see [19] for an extended review). Alternatively, nearshore bathymetry can be derived by video-based depth inversion, taking into account adequate error estimates [20]. Direct measurements through traditional acoustic surveys have a high resolution, but their application can be limited by logistic constraints and operating costs. Advances in the submarine monitoring of coastal areas came from the application of the Multibeam Echosounder System (MBES) to very shallow water areas, as well as by means of autonomous surface vehicles (ASVs) [21]. This technique allows the monitoring of submerged beaches with accuracy comparable to onshore in situ observations, and observing seabed changes commonly occurring in the extremely dynamic shoreface area.

In the framework of the *Strategie Innovative, Monitoraggio ed Analisi del Rischio Erosione* (STIMARE [22]) project, the southern coastal tract of Riccione has been selected for the application of integrated techniques of coastal monitoring (terrestrial laser scanner, GNSS, MBES). In this study, based on repeated surveys carried out in similar operative conditions in the emerged and submerged beach from November 2017 to February 2021, we describe the morphological evolution of the beach from a short-term (seasonal) to long-term (over a >3-year scale) time frame, with the aim of evaluating its overall response to the various interacting factors. The observed morphological changes are related to natural events (storm events, wave and current regime) and anthropogenic activities (beach sediment management, application of defense structures, nourishment interventions, etc.) carried out for reducing coastal erosion. The multitemporal monitoring involved both the emerged and submerged beach, providing evidence on the onshore–offshore sediment exchange in this periodically nourished beach and, in general, giving insight into the beach behavior with respect to the adopted management strategies.

2. The Study Site

2.1. General Setting and Coastal Dynamics

The beach under study is located in the Riccione Municipality, within a wider coastal macrocell (about 19 km) extending between Cattolica and Rimini, in the southernmost part of the Emilia-Romagna littoral area (Figure 1). The main drivers of changes at the decadal scale in this area are due to the predominant longshore current, directed from south to north, and the reduction in the local sediment supply since the 1950s [1]. Due to these factors, the southern area of this coastal cell underwent erosion (Cattolica, Misano, Riccione southern sector, Figure 1), while the northern tract, lying in the up-drift side with respect

to the Rimini jetty, gradually advanced. From Cattolica to Misano, the beach is protected by hard defense structures (groynes, breakwaters); the coastal stretch under study is in a down-drift position with respect to a series of hard structures protecting the beach of Misano (Figure 1) and this has consequences in terms of erosion in the southern Riccione area [23]. In the southern stretch of Riccione, instead of hard structures, a barrier made of sandbags and other experimental solutions (described in detail below) are used on the submerged beach to protect from coastal erosion. Misano and Riccione are periodically nourished by the Emilia-Romagna region in the framework of the "*Security projects through submarine sand nourishment for critical areas of the regional coastline*", such as in 2002, 2007 and 2016 [24].

Figure 1. Location of the study area (red rectangle) in the southernmost Emilia-Romagna coastal area (see inset). Black lines indicate the limits of municipalities; yellow lines represent the subdivision of littoral cells according to [24]. The studied area is part of cell 14 (shaded area). In the inset, location of the tide gauge at Marina di Ravenna and of the Nausicaa buoy at Cesenatico are indicated by a blue triangle and by a yellow dot, respectively. Orthophotograph is obtained from Agea 2011, while the image in the inset is derived from ESRI.

The beach of Riccione is an important touristic site during summer and is highly modified, with infrastructures such as a railway, highway and widespread touristic and recreational structures close to the coastal area. The beach stretch under study, about 400 m long, is located within cell 14, according to the littoral cell subdivision adopted for coastal management purposes [24], located northward of the Misano–Riccione boundary (Figure 1). In the southernmost tract of the Riccione Municipality, the beach is 60–120 m wide, with a maximum height of 1.5–1.8 m a.s.l. [1]. The sediments of the subaerial beach are mostly composed of fine sand (mean grain size: 0.205–0.180 mm), while on the submerged beach, the percentage of very fine sands increases (mean grain size 0.178–0.090 mm). Silt is present in small percentages only below a depth of 3 m. Clay is practically absent. Sediments are well sorted and moderately well sorted, apart from one poorly sorted sample (taken at a depth of 4 m). Overall, no relation between depth and sorting is observed.

Due to the wide touristic exploitation and the need to counteract coastal erosion problems, the evolution of the Emilia-Romagna coast has been monitored by Idroser (in 1984 and 1993, [25]) and, more regularly, by Arpae (in 2000, 2006, 2012, 2018 [1,26–28]). For the area under study in southern Riccione, the results of recent monitoring and volumetric change estimations show that the beach is in a state of erosion, although periodic nour-

ishment interventions are carried out to mitigate this tendency. From 1983 to 2018, over 1,680,000 m^3 of sand (about 48,000 m^3/yr) have been placed on this coastal area (cell 14 in Figure 1). In 2016, a major beach nourishment was undertaken at the regional scale, placing about 212,000 m^3 of sand dredged from the offshore in a 1400 m long coastal stretch of southern Riccione (Figure 2a). Based on post-nourishment surveys conducted by Arpae, which included the undersea beach where some of the sand was displaced, it was estimated that 66% of the total fill volume remained on the beach after the first two years [29,30].
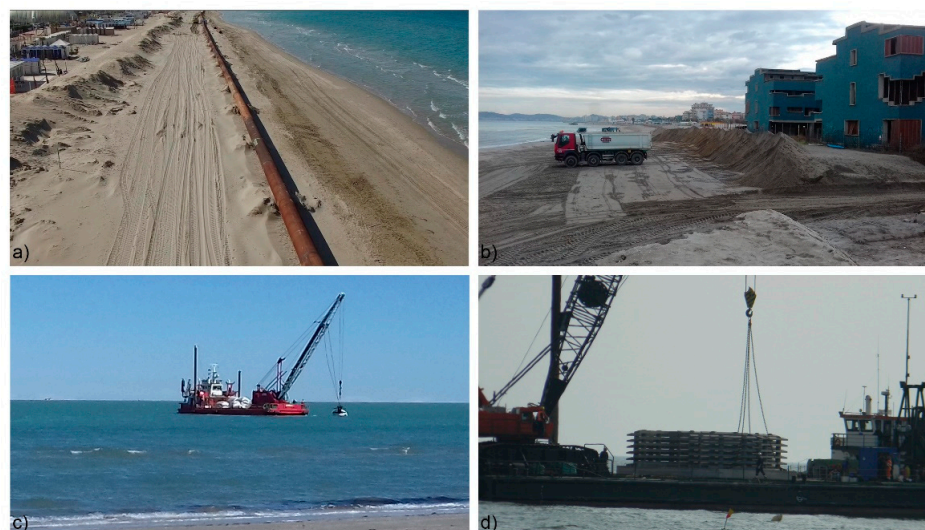

Figure 2. Interventions carried out on the emerged and submerged beach of Riccione: (**a**) replenishment operations in 2016; (**b**) creation of the artificial embankment in the backshore in winter; (**c**) periodical recharge of the sandbag barrier; (**d**) W-Mesh modules to be settled down on the seabed.

Moreover, as common practice before the winter season, large volumes of sediments are moved with trucks and excavators from the berm/intertidal zone (foreshore) toward the landward part of the beach. Here, an embankment some meters high is created, protecting the beach and the backshore from winter storms (Figure 2b). Before the summer, this embankment is gradually dismantled and the sediment is spread over the beach, where reshaping by beach resort license holders is a common activity. Another common activity in the beach sediment management is the "beach cleaning" carried out by local municipalities and beach resort license holders; the recovered sand can be used for nourishment purposes [24]. Available information regarding "seasonal" nourishment interventions and sediment movements carried out in the period of 2017 to the beginning of 2021, i.e., after the regional nourishment intervention of 2016, is given in Table A1. However, the volumes indicated for dumped sediments refer to the whole of cell 14 or part of it (not known) and not specifically to the beach stretch under study.

On the submerged beach, a 1000 m long barrier made of sandbags [23,31] was placed at about −2/−3 m, at a distance of about 150–180 m from the shoreline in 1983 [27], then was lengthened to a total length of 3000 m in 1995. It was designed to improve the durability of beach nourishment, carried out since 1983 in the Riccione coastal area. An analysis of the performance of this structure is given by [23]. Due to the poor resistance of the sandbags, the barrier is maintained through periodic recharge operations (Figure 2c). Moreover, in recent years, experimental structures made of concrete modular elements (called "W-Mesh", Figure 2d) designed with the purpose to enhance the wave energy dissipation and to reduce coastal erosion, have been installed on the seabed at a depth between −3.0 and −3.5 m offshore from the sandbag barrier (hereafter "area 1"). A first deployment of a few modules aimed to check the stability under operative conditions and took place in May 2017. In 2018, after some structural improvements, they were relocated

within "area 1", while in 2020 another 16 modules were installed just behind the sandbag barrier, at about −2.5 m ("area 2").

2.2. Meteo-Marine Climate

As commonly observed on the western coast of the Northern Adriatic Sea, the meteo-marine climate at Riccione is characterized by severe sea storms mainly generated by northeasterly winds, named Bora, although southeasterly winds, named Scirocco, may have relevant seasonal impacts [32,33]. The latter generally induces the highest surge levels, having much wider fetch than northeasterly winds [2]. For the Emilia-Romagna coast, wave and climate data are available, respectively, from the Nausicaa buoy and the meteorological station at Cesenatico (see Figure 1, inset for location). Nausicaa wave buoy data are available from May 2007, with a percentage of 86.1% of availability over 13 years, and are now the main source of information for the meteo-marine climate along the regional coast.

The wind distribution from the regional meteorological station, located at the Cesenatico harbor, is shown in Figure 3, where the polar distribution of the 10 min average hourly wind speed recorded at a height of 10 m is represented. Two main wind directions are evidenced, one from the northwest and one from the southeast, with the latter characterized by wind speed up to 15 m/s, while the sectors with larger frequencies of the higher wind speed are between 50° and 100° N.
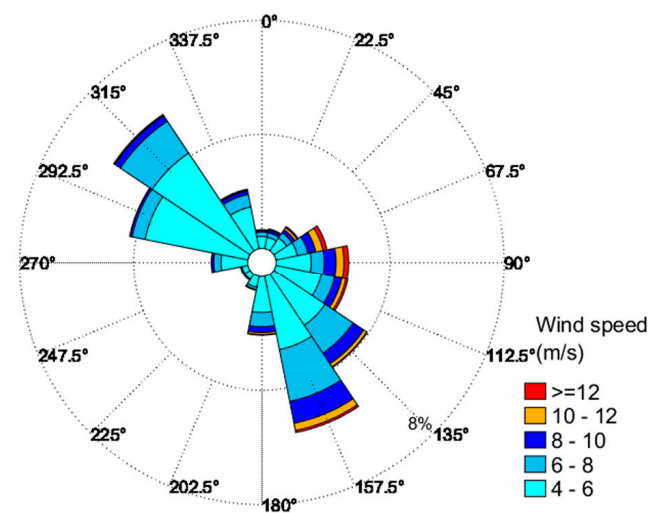

Figure 3. Wind regime at Cesenatico in the period 2010–2020: distribution of the 10 min average hourly wind speed at 10 m height.

The regional Nausicaa buoy is located off the coastline of Cesenatico (Figure 1) at a water depth of 10 m [34]. At this depth, refraction effects on the measured wave directions cannot be neglected, thus the recorded wave directions at Nausicaa are slightly bent towards the perpendicular contours, with the wave rays ranging approximately between 55° and 60° N.

The wave roses in Figure 4 represent the polar distribution of the significant wave height H_s (left panel) and the peak period T_p (right panel) versus the mean wave directions measured at the buoy, showing:

i.   the most energetic waves, up to 4.0 m in height, propagating from the sector 50°–60° N;
ii.   the most frequent conditions, with wave height up to 1.0 m, coming from 90° N;
iii.   the high wave periods with values ranging from 9–11 s, coming from 90° N;
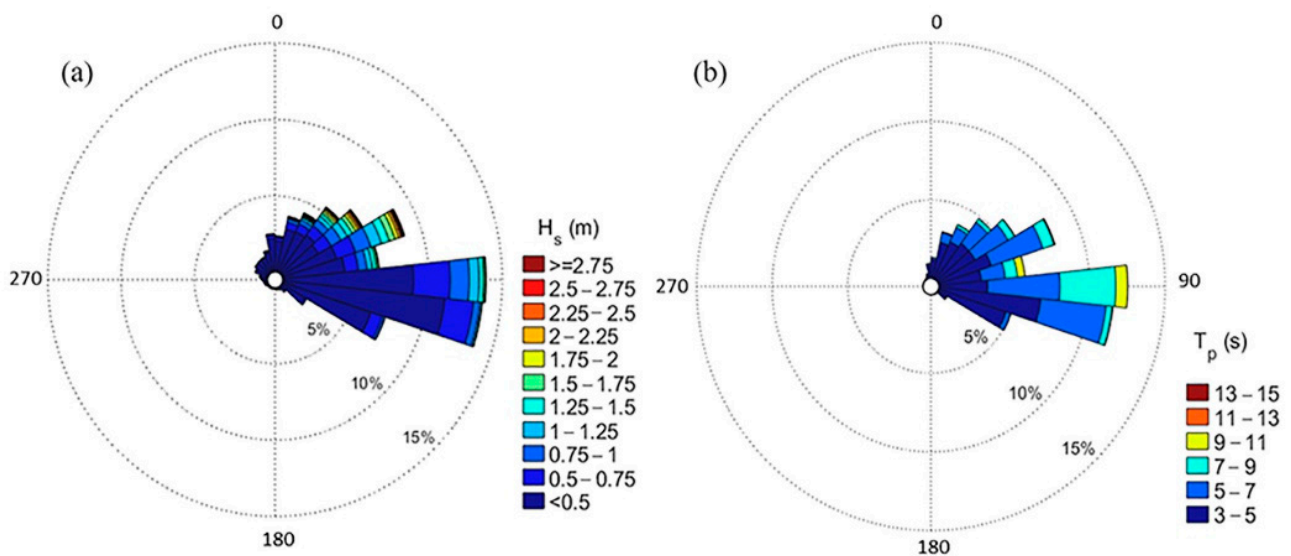iv.   the most frequent values of peak periods ranging from 5 to 7 s.

Figure 4. Wave regime from the Nausicaa buoy in the period 2010–2020: distribution with mean wave direction of (**a**) significant wave height (H_s) and (**b**) peak period (T_p).

Considering that the coastal stretch under study has a roughly NW–SE orientation, and that the perpendicular to the coast here is oriented about N 40–45°, the longshore current generated by the wave-breaking induced currents has a direction from southeast to northwest [1,28]; the associated average sediment transport in this coastal stretch was estimated through mono-dimensional numerical modeling in the range of 84–155 × 10^3 m^3/year [25].

In the Northern Adriatic Sea, the astronomical tide is characterized by mixed components that determine an excursion of about 30 cm in neap tides and 70 cm in spring tides [25]. However, storm surge levels due to water piling by prevailing winds and low barometric pressure may almost double the tidal range (extreme levels in the order of 1 m in the 1- to 10-year return period [35]) causing extensive inundation and erosion at the coast when associated with storm waves [2].

3. Data and Methods

3.1. Topographic–Bathymetric Surveys

Periodic topographic and bathymetric surveys were carried out by the University of Bologna, Department of Biological, Geological and Environmental Sciences (BiGeA) in a 400 m wide stretch of the Riccione beach (Figure 1) in the framework of the STIMARE project [22] from 2019 (Table 1). Due to limitations imposed by the COVID-19 pandemic situation and related difficulties in obtaining authorizations, surveys were suspended in 2020 and started again in 2021. Moreover, the data set includes the results of previous topo-bathymetric surveys carried out in the same area in November 2017 and November 2018 in the framework of Arpae monitoring activities (Table 1). All surveys were referenced through a global navigation satellite system (GNSS) based on RTK and network real-time kinematic (NRTK), providing measurements with a 5 cm error at most. For all the surveys (topographic and bathymetric), the same geodetic references have been used: ETRF2000-UTM32 (2008.0) (EPSG: 7791) as a planimetric reference system and the CARI0300 topographic benchmark of the Emilia-Romagna Coastal Geodetic Network (4877293.13N and 795374.49E; [1]) to obtain the orthometric height (m a.s.l.).

The first topographic survey in the framework of the STIMARE project was carried out on 24 May 2019, employing a terrestrial laser scanner (TLS) coupled with a GNSS-network real-time kinematic (NRTK) system for positioning a Leica Viva GS14 (Figure 5a). The same activity was carried out in the survey of 16–23 February 2021 (Table 1). The adopted TLS is a FARO Laser Scanner CAM2 Focus3D, based on "phase shift" technology, a system that allows it to reach a 6 mm resolution over a range of about 20 m [36].

Table 1. List of surveys carried out in the Riccione area.

Date	Kind of Survey	Project/Activity
28 November 2017	GNSS + MBES	Arpae monitoring
3 November 2018	GNSS + MBES	" "
24 May 2019	TLS + GNSS- + MBES	STIMARE project
6 December 2019	GNSS- + MBES	" "
16–23 February 2021	TLS + GNSS- + MBES	" "

Figure 5. (**a**) TSL survey; (**b**) ASV used for multibeam bathymetric surveys; (**c**) GNSS-NRTK system for positioning.

On 6 December 2019, for the emerged beach, a GNSS topographic survey was performed with a Leica Viva GS14 along 2 longshore transects, 4 cross-shore transects and a saw tooth shape/oblique transect, with points spaced approximately every 2 m. Data were processed with the appropriate transformations and corrections (reference system and orthometric height a.s.l.) to obtain a DTM gridded at 0.10×0.10 m, by means of generation of a triangulated irregular network (TIN) surface.

For the submerged beach, the 2019 surveys (May and December) were carried out using the same operating system, i.e., an autonomous surface vehicle (ASV) equipped with a PicoMB-120 multibeam system (MBES) (Figure 5b). This provided a complete bathymetric coverage from -0.4 m to $-4/5$ m of the studied area, with a vertical accuracy in the order of ± 5 cm. In the survey of February 2021, a Reson SeaBat 8125 MBES was used aboard a small vessel, to acquire bathymetry in the same area with a depth resolution of ± 3 cm. Data positioning in all surveys was GNSS-RTK by means of Trimble R7 and R8 receivers (Figure 5c). On the foreshore, the surveys were integrated with direct depth acquisition with GNSS-RTK on cross-shore transects in the first 0.4 m of depth.

All data for each survey were processed with dedicated software and merged in a single raster grid file, gridded at 0.10×0.10 m, suitable for geomorphologic and geomorphometric analysis in a GIS environment (Figure 6). Particular attention was given to the integration between the topographic and bathymetric surveys, in order to eliminate any possible errors related to the use of different methodologies [37,38].

Regarding the data acquired by Arpae in 2017 and 2018 (Table 1), it is important to point out that surveys were carried out with the same equipment and the data are considered fully comparable with those of subsequent surveys. In this case, point shapefiles with a resolution of 1 m were provided for the area. Similarly to the results of the other

surveys, the point shapefiles were firstly transformed in a TIN and then in a raster grid (Arc ASCII Grid).

3.2. DTM Geomorphologic Analysis

The DTMs resulting from the different surveys (Figure 6 and Table 1) were used for surface comparisons to evaluate geomorphological changes of the emerged and submerged beach. Height/depth changes were computed as the difference between a couple of successive DTMs. The resulting difference maps represent the surface change; in the case of a height increase or depth decrease, accretion due to sediment accumulation has occurred, while in the case of a height decrease or depth increase, sediment loss or erosion has occurred. The color scale in the difference maps considers ±0.1 m around 0 as a range of no significant change (to account for instrumental precision specifically given above) and then classes of ±0.2 m from values <−1 m and >1 m. The results of the three surveys that are close in time (November 2018, May and December 2019) were firstly compared, in order to demonstrate the evolution of the studied beach at the seasonal scale (Section 4.1). Furthermore, the comparison at the interannual scale among DTMs acquired in late autumn 2017 and 2018, late autumn–winter 2019 and winter 2021 is discussed (Section 4.2); this allows us to extend the analysis of the beach evolution to a wider time frame of >3 years. Finally, the overall evolution between the first and the last surveys, i.e., in the time frame November 2017–February 2021, is considered.

Beach profile comparison along selected sections obtained from the DTMs was also carried out, showing how the above described patterns of bathymetric changes in the DTMs are due to sediment reworking/accumulation and to local seabed erosion (Section 4.3).

Volumetric changes between different surveys were estimated from the previously described DTMs, resampled on a cell of 1 × 1 m, comparing the two analyzed surfaces of common areas and calculating the variation on the vertical (ΔZ) for each cell between the two surveys and multiplying it with the cell area. Positive and negative volume changes are thus obtained for each DTM comparison, representing accumulated or eroded sediment, respectively, and the final "net volume" is also given for the total surveyed area of 150,559 m^2. Combining uncertainties related both to the GNSS and to the echosounder, the variance in height estimation for each cell has been assumed as being equal to 5 cm to account for instrumental precision of the latter; the bias due to RTK was set to 1 cm. The overall associated uncertainty has been estimated according to [29], resulting in about 1560 m^3 equal to 1.04% in terms of volume uncertainty per square meter (m^3/m^2).

3.3. Analysis of Storm Events in the Studied Period

The available wave data recorded by the Nausicaa buoy [34] in the period of interest were analyzed. In order to characterize the extreme storm events in the monitoring time frame, and to relate the frequency and energy amount of these events with the morphological changes observed on the beach under study, the analysis of wave data was carried out for the period of 2017 to the beginning of 2021. According to [39], on the Emilia-Romagna coast, a sea storm is defined as an event characterized by a significant wave height higher than 1.5 m and lasting for at least 6 h. Two storms are then considered as separate events if the wave height decays below the above threshold for 3 or more consecutive hours.

The study of storm events was carried out with the calculation of the total energy (*E*) of each storm, identified through the integration of the significant height of the wave H$_s$ for the duration of the storm (dur), following the methodology of [40], which was subsequently adopted by [41,42] for local studies, to adapt the scale of ocean storms to the Mediterranean context, as:
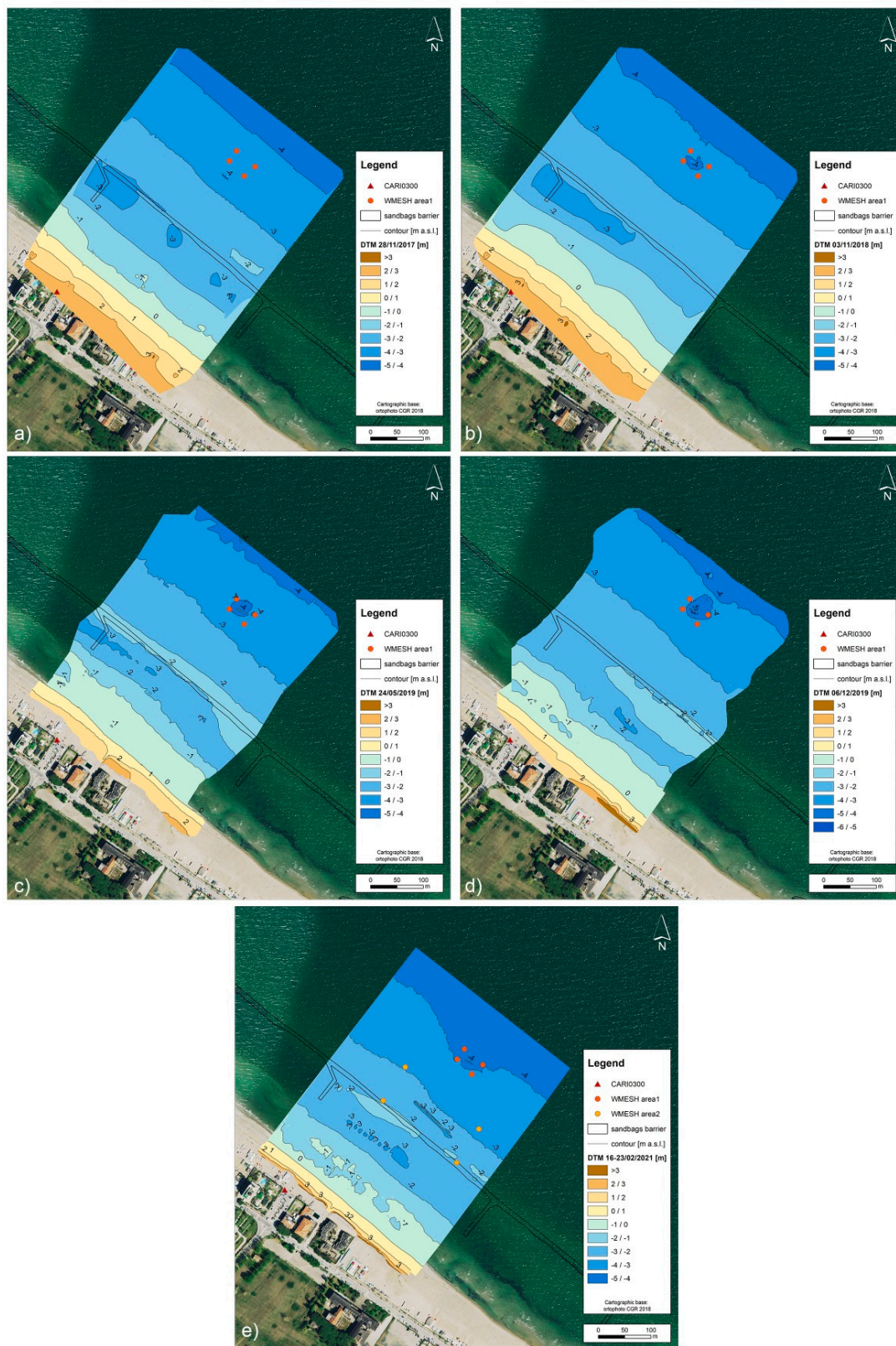
$$E = \int_{dur} H_s^2 dt \tag{1}$$

Figure 6. DTMs of the surveyed beach on: (**a**) 28 November 2017; (**b**) 3 November 2018; (**c**) 24 May 2019; (**d**) 6 December 2019; (**e**) 16–23 February 2021. The location of the submerged sandbag barrier, derived from aerial photographs [23], is indicated by black lines parallel to the beach at about -2 m. Red and orange dots indicate the areas of installation of W-Mesh structures (see text for details); the red triangle indicates the CARI0300 benchmark position on the backshore.

The event was then classified following [40] through the energy classification scale defining a storm as weak (class I) when $E \leq 58.4$ m^2 h, moderate (class II) when $58.4 < E \leq 127.9$ m^2 h, significant (class III) when $127.9 < E \leq 389.7$ m^2 h, severe (class IV) when $389.7 < E \leq 706.9$ m^2 h and extreme (class V) when $E > 706.9$ m^2 h. According to this classification, a list of events was compiled (Table A2), with the characteristics of the identified sea storms occurring in the period January 2017–February 2021.

Sea-level data were also analyzed in order to identify possible storm surge occurrence during storm events (Table A2). The maximum sea level as recorded at the Marina di Ravenna tide gauge (see Figure 1 for location), belonging to the national tide gauge network (RMN) of the National Institute for Research and Environment Protection (ISPRA), was collected for each storm event. These data are available with a certain temporal continuity from 1998, but with important gaps from 2015–2016 (availability less than 60%) and in 2018 (no data), with 77% availability over 11 years (i.e., 2010–2020).

4. Results

The DTMs obtained for the selected coastal area of Riccione are shown in Figure 6. The emerged beach was found to be about 40 to 80 m wide, with an average height of 0.8–1.1 m asl. Height values higher than 3 m are observed in the December 2019 and February 2021 surveys in the innermost sector of the beach (Figure 6d,e) corresponding to the artificial embankment built in winter for preventing flooding of the backshore during storms. The morphology of the submerged beach in the first few meters of depth is strongly controlled by the presence of the barrier made of sandbags lying about 170 m from the coastline, at a depth of around 2.5/3 m (Figure 6). The location indicated on the maps for the barrier represents its initial position, derived from aerial photographs [23]; then the barrier was partially buried by sediment and periodically recharged with new sandbags (Figure 2c). From the coast to the barrier, the seabed has an irregular shape, locally deepening to over -3 m, while it commonly shoals due to the barrier and to sediment accumulation close to it. This setting changes over time (Figure 6) as will be evidenced by the following DTM and beach profile comparisons (Sections 4.1–4.3). Beyond the barrier, the seabed gradually deepens to over -4 m with an average slope of 0.6°, the only irregularity being represented by some localized seabed deepening corresponding to the W-Mesh structures (area indicated by red and orange dots in Figure 6).

4.1. Seasonal Comparisons

A first seasonal comparison was carried out by taking into account the DTM of November 2018 with respect to the DTM of May 2019. The difference map (Figure 7a) shows a situation of prevalent accretion, both on the emerged and the submerged beach. Sediment accumulation on the emerged beach and on the nearshore is likely related to "ordinary" nourishment activities commonly carried out by the Civil Protection Agency in late spring (about 18,000 m^3 of sand used, Table A1). In particular, on the submerged beach, sediment accumulation with thickness up to >1 m is mostly concentrated along the sandbag barrier on both landward and seaward sides. Localized seabed deepening of up to -0.9 m occurs on the foreshore and nearshore. Diffuse seabed accretion in the order of $+0.1/0.3$ and $+0.3/0.5$ m is observed below a 3 m depth on most of the submerged beach, the only exception being around the W-Mesh structure, area 1, where localized lowering occurs (mostly in the order of $-0.1/0.3$ m, with values up to $-0.5/-0.7$ m).

The DTMs acquired in May and December, 2019 (Figure 6c,d) were then compared. Figure 7b shows the related topo-bathymetric difference map, which is markedly different from the previous November 2018–May 2019 intercomparison. The emerged beach, in fact, shows a diffused height decrease, likely due to artificial reshaping carried out to build up the winter embankment in the backshore (this feature was not surveyed, apart from a small part of its seaward edge at the southernmost limit of the map, where a sediment accumulation of >1.1 m is visible). Marked local bathymetric differences up to $+/-1$ m, both positive and negative, lie on the nearshore and close to the submerged barrier position,

where, in December, the location of the seabed deepening inside the barrier and beyond appears more extended with respect to May (see also 2D comparisons in Section 4.3). Conversely, sediment accumulation along the submerged barrier causes a depth decrease to less than −2 m (Figure 6c,d). In the DTM of December, this is located in an innermost, landward position with respect to May (Figure 6c,d). This "shift" clearly results in the difference map between the two surveys (Figure 7b), being reflected by parallel belts of local positive/negative bathymetric differences up to +/−1 m thick. On the rest of the submarine beach below −3 m, an overall relatively uniform, slight deepening of the seabed, in the order of −0.1/−0.3 m, is observed (locally up to −0.5 m in proximity to W-Mesh area 1).
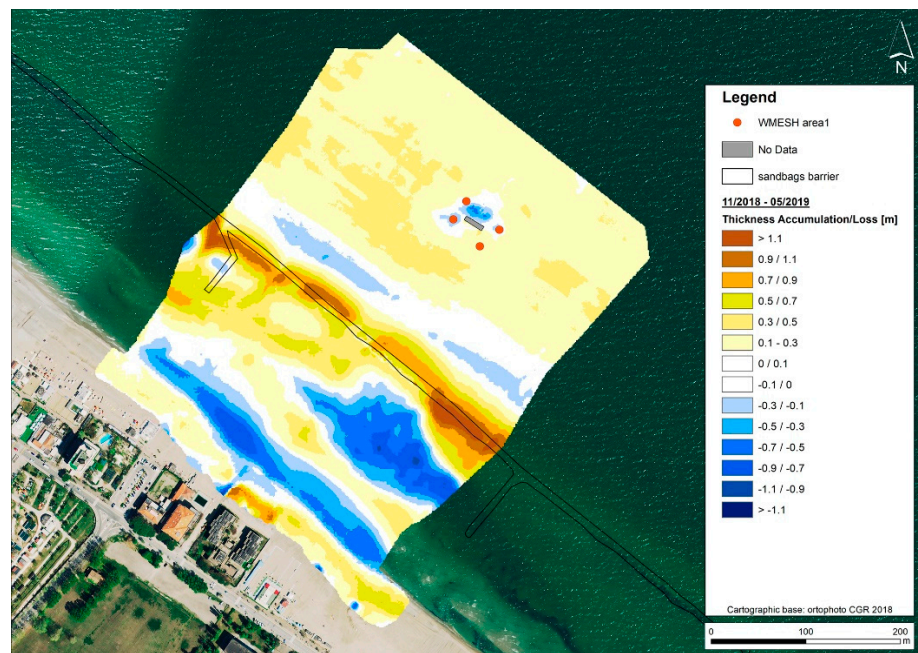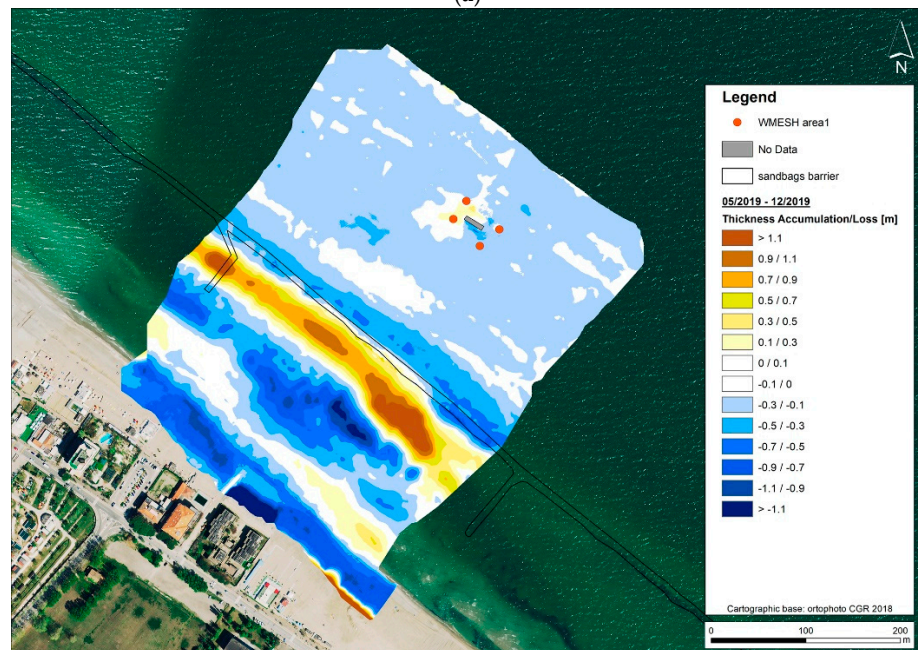
Figure 7. Difference maps between: (**a**) November 2018 and May 2019 DTMs; (**b**) May 2019 and December 2019 DTMs.

4.2. Interannual Comparisons

In this section, geomorphological changes at the interannual scale are considered, by comparing DTMs obtained from surveys carried out during late autumn–winter in a >3-year time frame.

The comparison between November 2017 and November 2018 surveys (Figure 8a) shows a modest but general height increment of tens of centimeters on most of the emerged beach. Alternating seabed accretion (mostly) and erosion occur on the submerged beach, both internally and externally to the submerged sandbag barrier. Beyond the barrier, apart from some NW–SE elongated negative differences in the bathymetry (in the order of −0.1/−0.3 m) parallel to this structure, and an expected localized, concentric seabed lowering/scouring at W-Mesh area 1, a general stability is observed in most of the submerged beach. A very localized, slight depth decrease to the southwest of W-Mesh area 1 is due to the relocation of the W-Mesh modules in 2018 with respect to their slightly landward position.

More intense morphological changes result from the November 2018–December 2019 DTMs comparison (Figure 8b). Height decreases up to −1.5 m are observed on the emerged beach and on the foreshore, likely partly due to sediment removal carried out for building up the winter embankment, which corresponds to a localized height increase in the SE-most area of the beach. On the inner nearshore, a diffused depth increase is also evident, with maximum seabed lowering up to −1.7 m localized in the central-southern part of the surveyed area. All along the inner (landward) side of the barrier, a continuous sediment accretion up to about +1.5 m is instead present (Figure 8b). Beyond the barrier and parallel to it, the seabed shows a slight deepening, in the order of −0.1/−0.3 m, as observed in the previous (2017–2018) comparison (Figure 8a). In the rest of the surveyed area below −3 m, a modest but generalized depth decrease (sediment accumulation with +0.1/0.3 m thickness) occurs. Again, a localized seabed lowering/scouring in the order of −0.3/−0.5 is visible around the W-Mesh structure.

The third interannual comparison (December 2019–February 2021, Figure 8c), with over 14 months of time lag, shows prevailing negative differences in the height/depth. Slight negative differences, corresponding to height decrease in the order −0.3/−0.1 m, are observed on the foreshore and on part of the emerged beach. On the nearshore, a marked NW–SE aligned depth increase to > −1 m is present in the central-southern part of the surveyed area, at an internal position with respect to the sandbag barrier. On the other side, only slight sediment accretion is observed on the nearshore and along the submerged barrier (Figure 8c). Beyond the barrier, a diffused seabed lowering of −0.1/−0.5 m is observed. While the seabed is relatively stable in terms of W-Mesh area 1, an extremely localized seabed scouring to over 1 m is visible along the new, NW–SE elongated W-Mesh structure installed in March 2020 (area 2 in Figure 8c).

Finally, the overall evolution in the >3-year long time frame between November 2017 and February 2021, revealed by morphological differences on the emerged and submerged beach, is shown in Figure 9. A height decrease up to >1 m is observed on the emerged beach and foreshore, apart from the accumulation of the winter embankment on the backshore that is not included in the survey area. Positive and negative alternating bathymetric differences, more or less parallel to the coastline (indicating loss and accumulation areas up to > −/+1 m) occur on the nearshore and close to the submerged barrier, respectively. Here, the sediment accumulation partly compensates for some local deepening of the seabed to over −3 m present in the November 2017 bathymetry on the inner side of the barrier (Figure 6a). A depth increase of −0.3/−0.7 m characterizes the submerged beach beyond the submerged barrier and, more slightly, the seabed below −3 m depth. Localized seabed lowering >−1 m appears in W-Mesh areas 1 and 2.
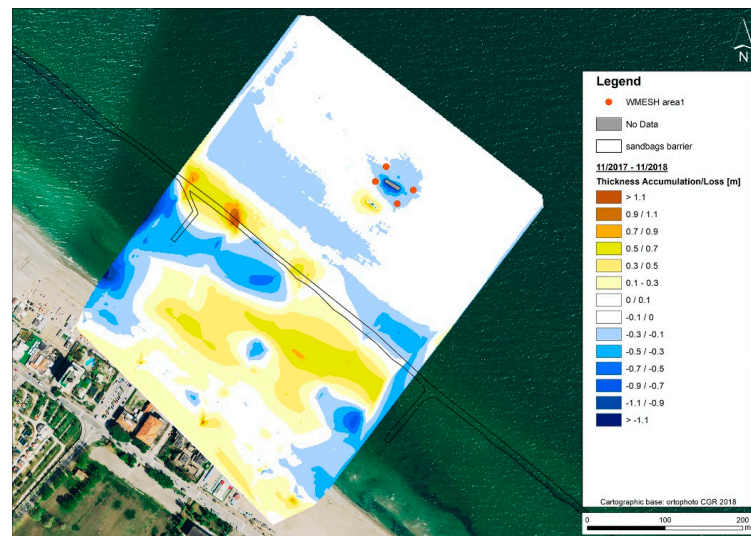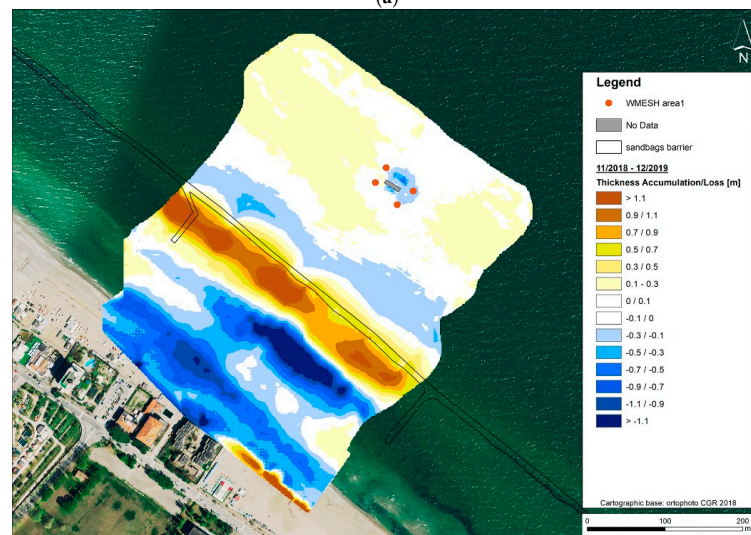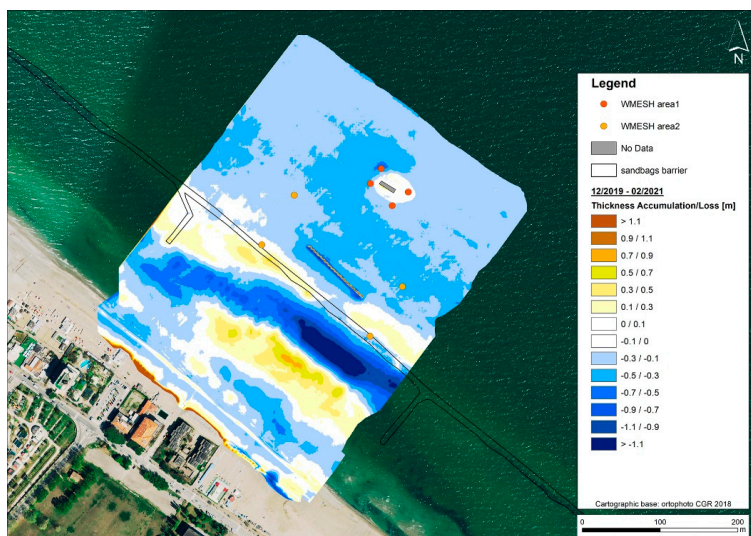
Figure 8. Difference maps between: (**a**) November 2017 and November 2018; (**b**) November 2018 and December 2019; (**c**) December 2019 and February 2021 DTMs.

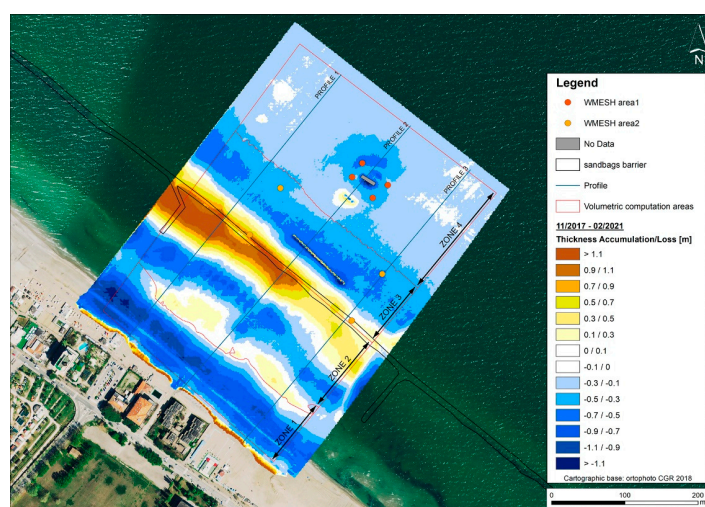**Figure 9.** Difference maps between November 2017 and February 2021 DTMs. The traces of the bathymetric profiles of Figure 10 and the subdivision in subzones selected for partial volumetric estimations are indicated.

4.3. 2D and Volumetric Comparisons

The analysis on difference maps was complemented by a 2D comparison of selected beach profiles, as shown in Figure 10. Sediment reworking and accumulation are observed at the submerged sandbag barrier, which is the most dynamic area in terms of sediment redistribution, both on the inner and the outer side with respect to its location (Figure 10). It has to be considered that the location indicated for the barrier on the maps (Figures 6–9) represents its original position, derived by aerial photographs [23]; then the barrier was partially buried under a natural bar [23], making it less visible. This is what we also observe in the bathymetric profiles of Figure 10. The W-Mesh modules are also indicated in Profile 2 of Figure 10 crossing these structures; they are associated with localized scouring in the seabed, as shown in the maps of Figures 8 and 9.

The volumetric difference estimates obtained by comparing successive DTMs were computed for the whole surveyed area and also for specific subzones, individuated on the basis of the dynamics observed in the above seasonal and interannual comparisons: "Zone 1" includes the backshore and the foreshore to the −1 m isobath, "Zone 2" includes the upper nearshore from the -1 m isobaths to the sandbag barrier, "Zone 3" includes the lower nearshore from the sandbag barrier to the −3 m isobath, "Zone 4" includes the offshore zone from the −3 m isobaths (Figure 9). The results of our estimations, rounded to the nearest ten, are summarized in Table 2, where the overall net volumetric variation ΔV for the whole area is also given.

The results for the whole surveyed area at the interannual scale show that in the case of the November/2017–November/2018 and November/2018–December/2019 intercomparisons, the estimated net volume difference is slightly positive (+5050 m^3) and slightly negative (−2830 m^3), respectively (Table 2), due to the fact that positive and negative volume differences (sediment gain and loss, respectively) are of comparable levels in those time frames. Conversely, large volumetric net differences occur at the seasonal scale in the November 2018–May 2019 DTM comparison (+21,000 m^3) and May/2019–December/2019 DTM comparison (−23,840 m^3) that, having an opposite tendency (overall positive/negative, respectively), compensate each other in the residual, slightly negative net volumetric difference at the interannual scale (comparison November 2018–December 2019) mentioned above. Larger negative volumetric changes are estimated, instead, for longer comparisons, such as the December 2019–February 2021 DTM difference (−32,290 m^3), as well as for the overall time frame of monitoring (November 2017–February 2021), resulting in a net volume loss of −30,080 m^3.
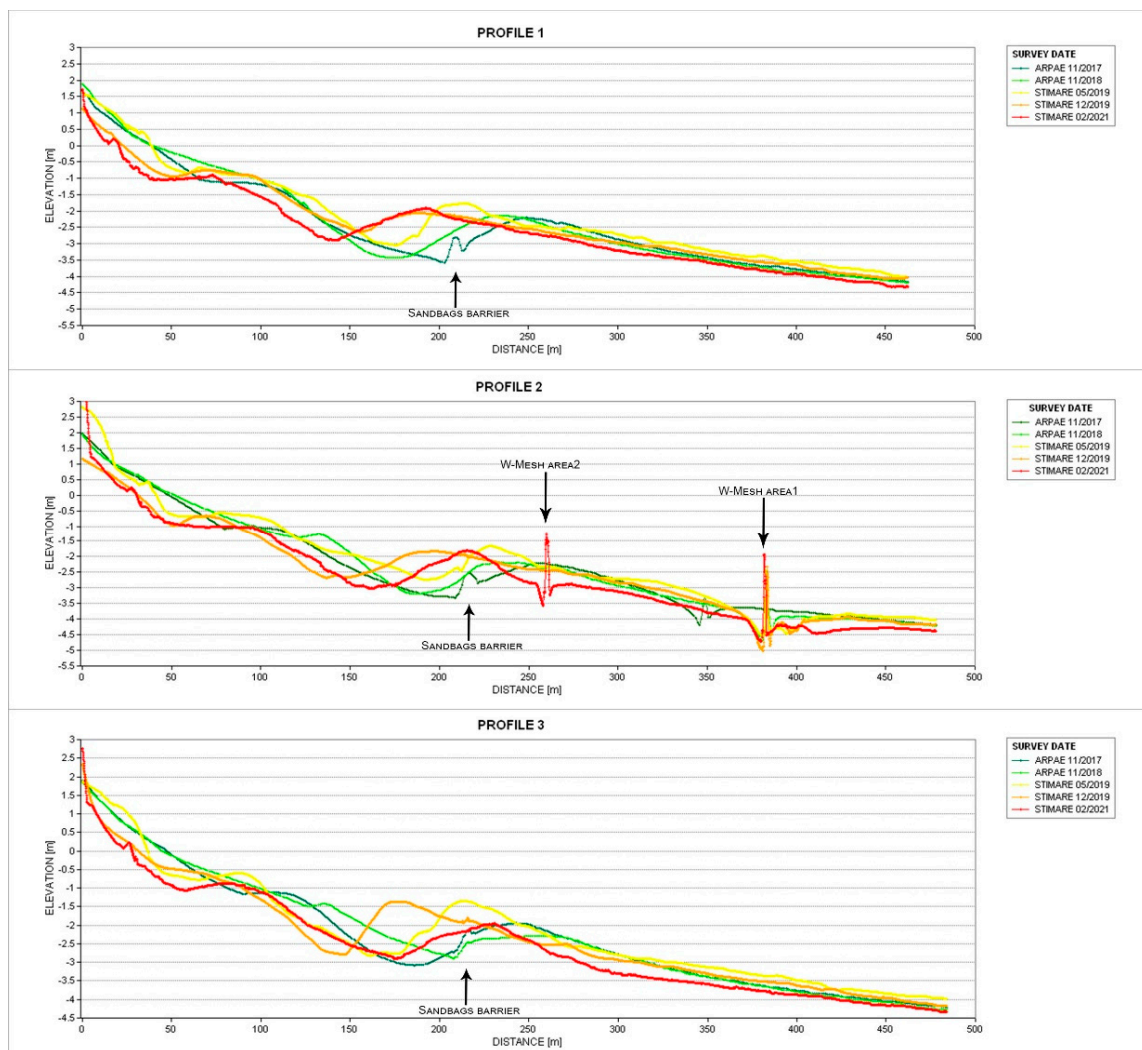
Figure 10. Beach section comparison along NE–SW oriented profiles (see Figure 9 for profile location). The position of the sandbag barrier and of the W-Mesh modules is indicated with arrows.

By observing in detail the volumetric differences estimated for each of the individuated subzones (Zone 1 to Zone 4 in Figure 9 and in Table 2), it appears that positive and negative differences are also locally relevant (sometimes compensating each other, such as in Zone 2) in specific subzones. Among these, the area close to the sandbag barrier, on the inner nearshore, shows the greatest volumetric and morphological variability.

These figures are discussed in Section 5 with regard to the beach morphological response to human interventions and natural processes. However, it is important to point out that the proposed volumetric estimations are not to be assumed to be a sedimentary budget balance for the surveyed area. To that purpose, an exhaustive inventory of sediment input and output items should be accounted for and considered at a larger scale (whole cell) while, for operative reasons due to the monitoring activities, the beach tract considered in morphologic analysis and volumetric estimates has a limited extension (about 400 m long alongshore), and it does not extend to the backshore and to a depth of more than 4 m.

4.4. Analysis of Seasonal Climate and Occurrence of Storm Events in the Studied Period

The analysis of seasonality in the time series of wave observations provides information on the intra-annual wave climate for each analyzed period; seasonal average wave height H_s and peak period T_p are plotted in Figure 11, together with their standard deviation. The panels show almost periodic signals, with sharp increments in wave height and

period during autumn and gradual drops during spring and summer. A similar seasonal-averaged wave climate characterized the four analyzed years, with a slight exception for 2020, when autumn and winter appear to be milder.

Table 2. Volumetric difference estimates among DTMs (in m^3).

Comparison		Interannual			Seasonal		Overall
		November 2017–November 2018	November 2018–December 2019	December 2019–February 2021	November 2018–May 2019	May 2019–December 2019	November 2017–February 2021
Zone 1	Volume difference	2370 −590	80 −11,290	170 −4210	1920 −5240	610 −8510	20 −13,520
	Net Δ Volume	1780	−11,220	−4050	−3320	−7900	−13,500
Zone 2	Volume difference	10,150 −3230	15,690 −11,340	4190 −12,580	11,180 −5650	9960 −11,140	10,720 −7850
	Net Δ Volume	6920	4350	−8390	5540	−1190	2880
Zone 3	Volume difference	2130 −3290	2370 −2800	510 −7000	7530 −890	40 −7050	2910 −10,910
	Net Δ Volume	−1150	−420	−6450	6640	−7010	−7990
Zone 4	Volume difference	320 −2770	4960 −410	60 −13,430	12,420 −210	130 −7790	80 −11,350
	Net Δ Volume	−2450	4550	−13,370	12,210	−7660	−11,270
Total area	Volume difference	14,950 −9900	23,060 −25,890	4920 −37,210	32,990 −11,990	10,750 −34,580	13,670 −43,750
	Net Δ Volume	5050	−2830	−32,290	21,000	−23,840	−30,080

The analysis of the identified storm events that occurred in the monitoring time frame (2017 to the beginning of 2021) shows that a total of 51 events occurred (Table A2). Of these, 9 events occurred in 2017, 15 in 2018, 13 in 2019 and 11 in 2020. Moreover, three events were recorded in the first two months of 2021. In detail, the annual percentage of sea storm events (Table 3) and the seasonal distribution of related energy (Figure 12) for complete years (2017 to 2020) indicate some differences among the years of observations:

- the year with the most energetic marine climate, with a total energy E equal to about 1600 m^2 h, was 2018, with a yearly occurrence of significant storms of 26.66%, mostly in winter;
- a higher amount of storm energy (E $\cong$ 900 m^2 h) occurred in winter 2017, when a severe storm, characterized by H_s > 4 m and duration > 3 days, was observed on January 17th;
- the year 2019 was overall a less energetic year in terms of storm energy (E $\cong$ 600 m^2 h), with a higher percentage (66.68%) of storms classified as weak. Most storm events occurred in spring (E $\cong$ 400 m^2 h);
- the year 2020 also shows a greater occurrence of storm events in spring (E = over 500 m^2 h);
- in all years, fewer and weaker sea storms were observed in summer, as expected.
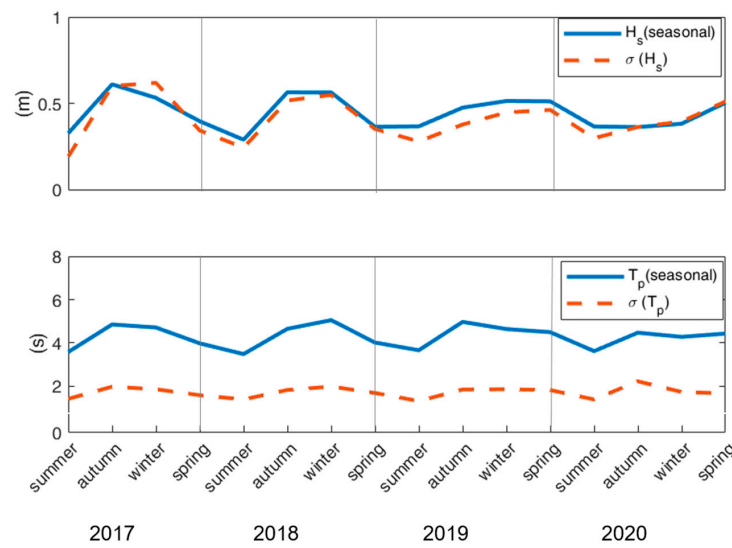
Figure 11. Seasonal distribution of the wave parameters in the years 2017–2020.

Table 3. Distribution of the sea storm events in the years 2017–2020 according to the energy classification.

	I—Weak	II—Moderate	III—Significant	IV—Severe
2017	44.45%	22.22%	22.22%	11.11%
2018	46.68%	26.66%	26.66%	0.00%
2019	66.68%	16.66%	16.66%	0.00%
2020	45.45%	36.37%	18.18%	0.00%

In the analyzed period, the sea water levels were higher or equal to 1.0 m only three times (October 2018, November and December 2019, see Table A2) and in all cases the associated sea storms were not strongly energetic, since they were classified in energetic classes I or II. However, the high storm surges associated with these storms induced flooding events all along the regional coast, causing significant damage to touristic structures and roads and collapsing of the artificial winter embankment, as witnessed by local media and direct observations by the authors.

In Section 5, we take into account and discuss the possible relation between the frequency and energy of storm events that occurred in the monitoring time frame and their integrated effect on the morphological changes observed on the beach under study.
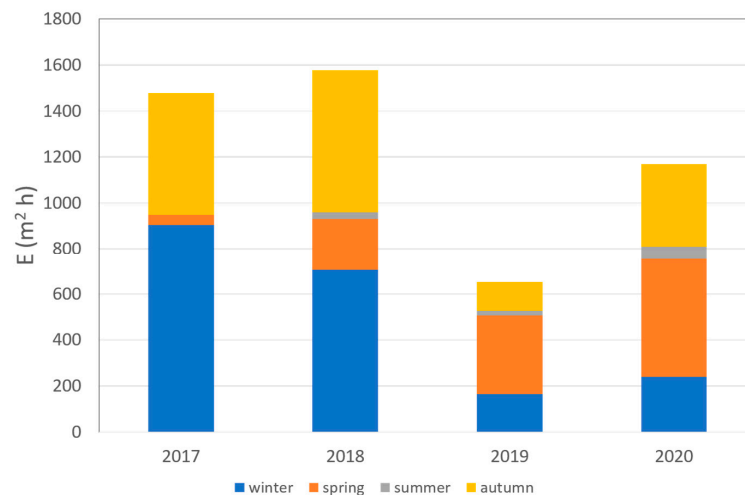

Figure 12. Seasonal distribution of the sea storm energy in the years 2017–2020.

5. Discussion

Accurate coastal monitoring and management require repetitive data collection, including bathymetric surveys that are essential for documenting the state and variability of the coast as a result of storms and other forcing factors [19]. Repeated topo-bathymetric monitoring of the emerged and submerged beach in the southern coastal tract of Riccione in a time frame of >3 years was carried out to observe the morphological evolution of the beach in relation to intervening factors. This coastal stretch is regularly nourished and protected with various interventions very close to each other, resulting in overlapping effects on the beach's morphological variations. These effects are hereafter discussed in terms of human interventions (Section 5.1) and of interplaying natural processes (Section 5.2).

5.1. Effects of Human Interventions on the Beach Morphology

Overall, the morphology of the southern Riccione beach is markedly influenced by human interventions, such as "common practices" in the beach sediment management and local interventions adopted to combat coastal erosion affecting this coastal stretch (see Section 2). On the emerged beach, in fact, sediments are commonly rearranged before winter by moving a consistent volume from the berm/intertidal zone to the backshore, to create the artificial winter embankment (Figure 2b). This activity accounts for the main observed morphological and volumetric changes observed here (Zone 1 in Table 2), such as in the November 2018–December 2019 DTM comparison.

Nourishment interventions are managed at the regional scale, such as in 2002, 2007 and 2016 along several parts of the Emilia-Romagna coast (including southern Riccione) with submarine sand [29,43], and as small-scale "maintenance replenishments" carried out by the Civil Protection Agency (Table A1). In this case, sediment can be of external provenance, such as from nearby coastal cells or construction excavations, or it may derive from the beach cleaning operations of the southern Riccione beach itself. In any case, nourishment provides a net sediment input that is crucial in facing erosion, considering that almost no natural sources of fluvial sediment supply are present in this macrocell. The positive effect of the 2016 main nourishment intervention of about 212,000 m^3 and of other minor interventions (Table A1) probably explains the overall relative stability and slight volumetric changes observed in the surveyed area at the interannual scale in the November 2017–November 2018 and November 2018–December 2019 comparisons (Table 2). Sediment accumulation on the foreshore and the nearshore in these time frames can be linked to the redistribution of dumped sediment after the 2016 major nourishment intervention, as pointed out by [1]. In the first post-nourishment monitoring in November 2017 (1.5 year after the nourishment intervention), in fact, the gradual sediment redistribution from the emerged (over $-65,000$ m^3 of sand displaced) to the submerged beach (where about 70,000 m^3 was deposited at the sandbag barrier, see also Figure 10) and to nearby beach sectors (some 24,000 m^3) was evidenced. Further surveys carried out by Arpae in the first two years after the 2016 nourishment estimated that about 66% of the total fill material was still present on this coastal stretch [29,30].

On the submerged beach, the presence of the sandbag barrier at about a 2 m depth causes a marked interference in the sediment transport, both in the cross-shore and in the longshore direction, as previously observed in all post-nourishment monitoring activities [23,29–31,43,44]. Sediment accumulation was frequently observed seaward of the barrier and localized erosion landward of it, where local seabed lowering to -4 m was frequently observed [30,31]. Our later monitoring activity, carried out in the time frame of 2017–2021, again showed the marked mobility of sediment in the sandbag barrier area (Figures 7–10 and Zone 2 in Table 2). Overall, this structure appears to stabilize the formation of the natural sand bar [23,31,44] that gradually migrates in the cross-shore direction. Moreover, according to [30,44], part of the sand volume estimated on the southern Riccione beach in 2017 was likely transported here by the N-ward longshore current from the nearby dumping site of Misano, also suggesting a role of the submerged barrier in intercepting the littoral drift. An analysis of the performance of this structure is given in [23] and goes be-

yond the purpose of this work, however, the effects of the sandbag barrier on the sediment deposit should also be evaluated in future post-nourishment monitoring activities.

The presence of experimental coastal defense structures in the study area (W-Mesh modules) has localized scouring effects on the submerged beach (Figures 7–10); due to their limited extension and few monitoring data, their efficiency in reducing wave impact at the coast is difficult to evaluate. However, the recent location of the new W-Mesh modules close to the sandbag barrier is considered inappropriate, and continuous monitoring of their effects on the seabed is strongly recommended.

5.2. The Contribution of Natural Processes

Due to the extensive human activities influencing the beach's morphological behavior, the effects of natural processes, such as in response to the annual and seasonal wave regime and littoral currents, are more difficult to appreciate. At the interannual scale, the morphological response of the beach recorded at the time of winter surveys (November 2017 and 2018, December 2019, February 2020 and February 2021) is quite different over time. Besides the common effects on the emerged and submerged beach due to the human factors cited in Section 5.1, producing alternating localized erosion and deposition areas, especially in the foreshore and at the submerged barrier (Figures 7–10 and Table 2), the beach's response may be due to a different annual wave regime and to the occurrence of storm surge events. For instance, the total sediment loss (over $-30,000$ m^3 in both cases) estimated for the December 2019–February 2021 interval (Figure 8 and Table 2) and for the overall November 2017–February 2021 time frame (Figure 9), the latter resulting from cumulative effects over the whole monitoring period, may be related to the contribution of natural processes. The occurrence of a significant storm (degree III, with a high degree of energy, see Table A2) on 14 February 2021, i.e., two days before the survey, might have resulted in the generalized seabed erosion recognized in the surveyed beach morphology at that time (Figures 6c, 8c and 10) and volumetric negative differences on the emerged and submerged beach (Table 2).

The effects of natural processes are quite evident in the seasonal intercomparisons of the 2019 surveys. In the November 2018–May 2019 DTM comparison (Figures 6b and 10), a situation of prevalent aggradation is present both on the emerged and on the submerged beach. The estimated high positive volumetric difference ($+21,000$ m^3, Table 2) in this time frame can be mostly explained by taking into account the contribution of repeated nourishment activities on the beach (about 18,000 m^3 of sand in March–May 2019 period, Table A1) and the sediment exchange between the emerged and the submerged beach, as discussed in Section 5.1 (see Figures 9 and 10). This may have resulted in the diffused seabed accretion observed on most of the submerged beach below a 3 m depth (Figures 6b and 10), similarly to what was observed in the beach monitoring carried out ~2 years after the 2002 "regional-scale" nourishment intervention at Riccione [44]. Natural processes may have favored this condition; the year 2019 was the least energetic in terms of storm energy in the study period (see Section 4.3), with most storms classified as weak, and the relatively more energetic storm events occurring in springtime (two of them in May 2019; see Table A2). In particular, the occurrence of a class III storm about a dozen days before the survey of May 2019 (Table A2) could have promoted the sediment migration and redistribution toward the submerged beach as well as beyond the sand barrier and on the offshore.

This situation was completely different at the time of the following survey (December 2019, Figure 6b), when a generalized seabed lowering with respect to May 2019 is recognized (Figure 10), apart from a localized sediment accumulation in the inner nearshore, internal to the submerged barrier, in the central-southern part of the surveyed area. Summer and autumn 2019 (see Table A2 and Figure 12) were the less energetic in terms of storm energy in the whole of the examined period. However, November 2019 was characterized by repeated storm surge events in the Northern Adriatic area (see, for instance, the November 12–13 extreme event that caused significant damage, especially in Venice, [45]); two

wave storm events associated with high storm surges (November 17 and 24, see Table A2) are recorded here. This probably explains the overall negative estimated net volumetric difference in the May–December 2019 DTM comparison ($-23,840$ m^3). This figure roughly balances the positive volumetric changes ($+21,000$ m^3) estimated for the preceding November 2018–May 2019 DTM comparison, resulting in the slight negative net volume difference (-2830 m^3) in the interannual time frame (November 2018–December 2019, Table 2). These data also clearly indicate that the interannual comparisons represent cumulative results and are thus not representative of the short-term and mid-term beach evolution, and point to the need for repeated, seasonal monitoring activities.

6. Conclusions

The morphological evolution of the emerged and submerged southern Riccione beach, where different coastal management strategies to reduce coastal erosion are adopted, is strongly influenced by anthropogenic activities, overlapping natural processes in the beach morphological response. On the subaerial beach, the frequent artificial reshaping of the beach redefines the beach morphology almost continuously. Nourishment interventions, carried out here on a more or less regular basis since 1983, provide a temporary sediment input to counteract the natural sediment deficit and coastal erosion trends, but require regular maintenance (and possibly subsequent monitoring) to be mostly effective. The overall tendency observed in the >3-year time frame of our monitoring suggests, in this regard, that the positive effect of the 2016 nourishment intervention carried out on the southern Riccione beach is gradually vanishing.

On the submerged beach under study, greater morphological dynamism is observed at the sandbag barrier, both on the land side and the sea side, where a marked interference with the sediment transport on the foreshore, both in the cross-shore and in the longshore direction, is observed. This effect is particularly evident in monitoring activities carried out on the beach after major nourishment interventions [29,30,43] and provides an interesting indication of the role of this structure in intercepting sediment on the nearshore and favoring the formation of the natural bar. On the other side, localized seabed scouring affects the areas where experimental structures (i.e., W-Mesh modules) have been placed on the submerged beach. Furthermore, the partial overlapping of the different interventions adopted to combat erosion, as they are close to each other (such as the recent installation of W-Mesh in area 2, in close proximity to the sandbags barrier), makes it difficult to evaluate their effects. This points to the need for a more integrated, well-designed approach for interventions at the coast, integrated with monitoring activities carried out on a regular basis. Our study demonstrates the applicability of an integrated monitoring of the emerged and submerged beach to this purpose.

The study case in southern Riccione attests to how much human intervention can alter sediment transport dynamics, disrupting natural beach behavior, as also observed elsewhere [11], where the dynamic interaction between natural and human processes needs to be balanced in a sustainable strategy view. At Riccione, the effectiveness of the adopted interventions to combat erosion appears to be not fully successful in the presence of an overall sediment deficit at the coast. This attests to the need for repeated and adequate nourishment interventions, and a correct management of the "sediment resource", in order to maintain this coastal tract in an equilibrium condition [24,29]. A long-term and holistic view of coastal management and defense strategies, also involving stakeholders and local institutions, is particularly important in the view of climate change consequences, since highly urbanized and low-lying coasts suffering from erosion, such as the southern Riccione beach, will be particularly susceptible to the impacts of climate change-related effects.

Author Contributions: Conceptualization, C.R.; methodology, C.R., L.C., F.S., N.D.N., M.M., M.A., M.G.G. and R.A.; software, F.S., L.C. and N.D.N.; validation, L.C., F.S., N.D.N. and M.G.G.; formal analysis, C.R., F.S., N.D.N. and M.G.G.; investigation, C.R., L.C., F.S., N.D.N., M.M., M.A., M.G.G. and R.A.; resources, C.R., L.C., N.D.N., M.M. and M.A; data curation, F.S., L.C., M.G.G. and N.D.N.; writing—original draft preparation, C.R., F.S. and M.G.G.; writing—review and editing, R.A., N.D.N.,

Appendix A

Table A1. Nourishment intervention carried out in the period of 2017 to the beginning of 2021 in cell 14 in southern Riccione extending northward from the Misano–Riccione boundary, for a total length of 1 km (see Figure 1). It is important to note that the studied coastal tract (about 400 m long, red box in Figure 1), is just a part of cell 14. The volumes indicated for dumped sediments (courtesy of Civil Protection Agency, Rimini) are thus only indicative, since they refer to the whole cell or part of it (not known) and not specifically to the beach tract under study. The provenance from other coastal tracts or from cell 14 is indicated in brackets (cell number from [24]), as well as provenance from land (construction excavations). The dates of the surveys carried out in the area are also indicated.

Year	Month	Dumped Volumes (m^3)	Nourishment Location	Provenance (n. cell)
2017	April	4200	emerged beach	Miramare (24)
	28 November 2017—1° survey (Arpae)			
2018	May	5428	-	Miramare (24)
	May	2000	-	Riccione S beach cleaning (14)
	3 November 2018—2° survey (Arpae)			
2019	March	7520	emerged beach	Miramare (24)
	May	6060	emerged beach	Miramare (24)
	May	4640	emerged beach	Riccione S beach cleaning
	24 May 2019—3° survey (STIMARE)			
	6 December 2019—4° survey (STIMARE)			
	December	2000	emerged beach	Misano (12)
2020	October	-	winter dune	Riccione south berm
	December	8500	emerged beach	Construction excavations
2021	February	2500	emerged beach	Miramare (24)
	16–23 February 2021—5° survey (STIMARE)			

Table A2. Sea storm events occurring in the period 2017–2021: wave significant height (H_s), mean (T_m) and peak (T_p) wave period, mean wave direction (MWD), compass sector, storm duration (dur), storm energy (E), energetic class, max sea level at Ravenna or Porto Garibaldi (in gray). (a) Sea level data not available at Ravenna or Porto Garibaldi; (b) Nausicaa data not available. The timing of the bathymetry surveys performed in the studied area is also indicated.

Year	Date	Season	H_s (m)	T_m (s)	T_p (s)	MWD (°N)	Compass Sector	Dur (h)	E (m² h)	Class	Max Level (m)
2017	6-January-17	winter	2.75	5.6	7.7	58	I	45	220.5	III	0.15
	17-January-17	winter	4.18	6.1	8.3	58	I	96	619.9	IV	0.55
	6-February-17	winter	2.01	5.3	7.7	79	I	8	24.7	I	0.45
	25-February-17	winter	3.08	5.5	7.1	49	I	8	38.4	I	0.44
	18-April-17	spring	2.94	5.3	6.7	32	I	9	45.3	I	0.41
	6-November-17	autumn	2.79	5.6	8.3	61	I	19.5	89.68	II	0.83
	13-November-17	autumn	3.68	6.7	9.1	59	I	50.5	302.96	III	0.93
	26-November-17	autumn	3.07	5	7.7	46	I	11	50.77	I	0.36
	28-November-17					Bathymetric survey					
	2-December-17	autumn	2.39	5.3	7.7	58	I	22	86.48	II	0.69
2018	3-February-18	winter	2.51	5.3	8.3	55	I	9.5	36.15	I	0.70
	13-February-18	winter	1.78	4.4	6.2	24	I	7	20.33	I	0.52
	18-February-18	winter	2.70	5.6	8.3	59	I	15	70.10	II	0.45
	24-February-18	winter	3.00	6	8.3	75	I	67.5	331.37	III	0.70
	26-February-18	winter	2.49	5.5	7.1	48	I	59	248.20	III	0.61
	21-March-18	spring	3.10	6	9.1	65	I	37	182.44	III	0.83
	23-March-18	spring	2.13	5.1	7.1	42	I	12.5	42.66	I	0.72
	26-August-18	summer	2.00	5.1	7.7	37	I	9	28.14	I	0.53
	24-September-18	autumn	2.75	5.8	8.3	316	IV	47	188.87	III	0.59
	2-October-18	autumn	2.36	5.3	7.7	23	I	11.5	49.20	I	0.40
	21-October-18	autumn	2.76	5.6	7.1	340	IV	20	73.58	II	0.57
	29-October-18	autumn	2.63	6.2	9.1	46	I	16.5	75.98	II	1.06
	3-November-18					Bathymetric survey					
	17-November-18	autumn	2.33	5.5	7.7	44	I	34.5	121.52	II	(a)
	20-November-18	autumn	2.66	5.4	7.7	42	I	11.5	55.93	I	(a)
	27-November-18	autumn	2.3	5.1	6.2	66	I	16.5	53.12	I	(a)

Table A2. *Cont.*

Year	Date	Season	H_s (m)	T_m (s)	T_p (s)	MWD (°N)	Compass Sector	Dur (h)	E (m² h)	Class	Max Level (m)
2019	23-February-19	winter	2.84	6.1	9.1	66	I	32	145.29	III	0.12
	20-March-19	winter	1.89	4.8	7.1	63	I	6.5	20.10	I	0.31
	26-March-19	spring	3.6	6.3	8.3	38	I	7.5	67.50	II	0.73
	4-April-19	spring	1.94	6.2	9.1	82	I	8	22.13	I	0.73
	5-May-19	spring	2.77	5.6	7.1	52	I	19.5	80.04	II	0.65
	12-May-19	spring	2.75	5.3	7.1	32	I	31	143.70	III	0.46
	14-May-19	spring	2.02	4.9	6.7	38	I	23.5	28.65	I	0.38
	24-May-19					Bathymetric survey					
	3-September-19	summer	1.85	4.8	6.7	55	I	6.5	18.8	I	0.49
	3-October-19	autumn	2.5	5.4	7.7	28	I	9	38.4	I	0.59
	17-November-19	autumn	1.87	6.5	9.1	83	I	7.5	22.8	I	1.11
	24-November-19	autumn	1.77	5.5	8.3	82	I	13.5	34.8	I	0.86
	6-December-19					Bathymetric survey					
	10-December-19	autumn	1.75	5.1	6.7	66	I	11	30.9	I	0.30
	23-December-19	winter					(b)				1.0
2020	20-January-20	winter	1.73	4.7	5.9	61	I	21	55.1	I	0.27
	6-February-20	winter	2.54	5.3	7.1	44	I	18.5	84.1	II	0.34
	25-March-20	spring	4.05	7.8	25	58	I	76.5	369.6	III	0.32
	31-March-20	spring	2.24	5.2	7.1	48	I	17	56.0	I	0.32
	1-April-20	spring	1.88	4.7	6.2	61	I	10.5	29.9	I	0.17
	14-April-20	spring	2.58	5.5	7.7	59	I	16	58.5	II	0.22
	7-July 20	summer	3.06	6.0	8.3	59	I	9	54.4	I	0.29
	28-September-20	autumn	1.72	4.3	5.9	21	I	11	30.0	I	0.58
	21-November-20	autumn	2.93	6.0	8.3	58	I	41	257.6	III	0.46
	5-December-20	autumn	1.91	5.6	9.1	84	I	27	73.0	II	0.85
	26-December-20	winter	2.60	5.6	7.7	55	I	28	101.0	II	0.52
2021	11-February-21	winter	1.80	4.7	6.7	63	I	8.0	22.4	I	0.60
	14-February-21	winter	2.57	5.1	7.1	32	I	41.5	196.6	III	0.46
	16-February-21					Bathymetric survey					
	27-February-21	winter	2.22	5.2	7.1	68	I	14.5	45.6	I	0.28

References

1. Arpae. Stato del Litorale Emiliano-Romagnolo al 2018. Erosione e interventi di difesa. In *I Quaderni di Arpae*; Aguzzi, M., Costantino, R., De Nigris, N., Morelli, M., Romagnoli, C., Unguendoli, S., Vecchi, E., Eds.; Arpae Emilia Romagna: Bologna, Italy, 2020; p. 224. ISBN 978-88-87854-48-0. Available online: https://www.arpae.it/it/notizie/slem-2018.pdf (accessed on 20 February 2021).
2. Armaroli, C.; Ciavola, P.; Perini, L.; Calabrese, L.; Lorito, S.; Valentini, A.; Masina, M. Critical storm thresholds for significant morphological changes and damage along the Emilia-Romagna coastline, Italy. *Geomorphology* **2012**, *143–144*, 34–51. [CrossRef]
3. Perini, L.; Calabrese, L.; Salerno, G.; Ciavola, P.; Armaroli, C.G. Evaluation of coastal vulnerability to flooding: Comparison of two different methods adopted by the Emilia-Romagna region (Italy). *Nat. Hazards Earth Syst. Sci.* **2016**, *16*, 181–194. [CrossRef]
4. Perini, L.; Calabrese, L.; Luciani, P.; Olivieri, M.; Galassi, G.; Spada, G. Sea-level rise along the Emilia-Romagna coast (North-ern Italy) in 2100: Scenarios and impacts. *Nat. Hazards Earth Syst. Sci.* **2017**, *17*, 2271–2287. [CrossRef]
5. MATTM-Regioni. Linee Guida Nazionali per la Difesa della Costa dai Fenomeni di Erosione e Dagli Effetti dei Cambiamenti climatici. Documento Elaborato Dal Tavolo Nazionale Sull'erosione Costiera, MATTM-Regioni col Coordinamento Tecnico di ISPRA. 2018, p. 305. Available online: http://www.erosionecostiera.isprambiente.it/files/linee-guida-nazionali/TNEC_LineeGuidaerosionecostiera_2018.pdf (accessed on 10 November 2019).
6. Haxel, J.H.; Holman, R.A. The sediment response of a dissipative beach to variations in wave climate. *Mar. Geol.* **2004**, *206*, 73–99. [CrossRef]
7. Vousdoukas, M.I.; Almeida, L.P.M.; Ferreira, O. Beach erosion and recovery during consecutive storms at a steep-sloping, meso-tidal beach. *Earth Surf. Process. Landf.* **2011**, *37*, 583–593. [CrossRef]
8. Ruggiero, P.; Kaminsky, G.M.; Gelfenbaum, G.; Cohn, N. Morphodynamics of prograding beaches: A synthesis of seasonal-to-century-scale observations of the Columbia River littoral cell. *Mar. Geol.* **2016**, *376*, 51–68. [CrossRef]
9. Makar, A.; Specht, C.; Specht, M.; Dąbrowski, P.; Burdziakowski, P.; Lewicka, O. Seabed Topography Changes in the Sopot Pier Zone in 2010–2018 Influenced by Tombolo Phenomenon. *Sensors* **2020**, *20*, 6061. [CrossRef] [PubMed]
10. Pietro, L.S.; O'Neal, M.A.; Puleo, J.A. Developing Terrestrial-LIDAR-Based Digital Elevation Models for Monitoring Beach Nourishment Performance. *J. Coast. Res.* **2008**, *246*, 1555–1564. [CrossRef]
11. Hein, C.J.; Fallon, A.R.; Rosen, P.; Hoagland, P.; Georgiou, I.Y.; FitzGerald, D.M.; Morris, M.; Baker, S.; Marino, G.B.; Fitz-simons, G. Shoreline Dynamics Along a Developed River Mouth Barrier Island: Multi-Decadal Cycles of Erosion and Event-Driven Mitigation. *Front. Earth Sci.* **2019**, *7*, 103. [CrossRef]
12. Bonaldo, D.; Antonioli, F.; Archetti, R.; Bezzi, A.; Correggiari, A.; Davolio, S.; De Falco, G.; Fantini, M.; Fontolan, G.; Furlani, S.; et al. Integrating multidisciplinary instruments for assessing coastal vulnerability to erosion and sea level rise: Lessons and challenges from the Adriatic Sea, Italy. *J. Coast. Conserv.* **2019**, *23*, 19–37. [CrossRef]
13. Casella, E.; Rovere, M.; Pedroncini, A.; Stark, C.; Casella, M.; Ferrari, M.; Firpo, M. Drone as a tool for monitoring beach to-pography changes in the Ligurian Sea (NW Mediterranean). *Geo-Mar. Lett.* **2016**, *201636*, 151–163. [CrossRef]
14. Hodúl, M.; Bird, S.; Knudby, A.; Chénier, R. Satellite derived photogrammetric bathymetry. *ISPRS J. Photogramm. Remote. Sens.* **2018**, *142*, 268–277. [CrossRef]
15. Almar, R.; Bergsma, E.W.J.; Maisongrande, P.; Melo de Almeida, L.P. Wave-derived coastal bathymetry from satellite video imagery: A showcase with Pleiades persistent mode. *Remote. Sens. Environ.* **2019**, *231*, 111263. [CrossRef]
16. Turner, I.L.; Harley, M.D.; Almar Erwin, R.; Bergsma, W.J. Satellite optical imagery in Coastal Engineering. *Coast. Eng.* **2021**, *167*, 103919. [CrossRef]
17. Klemas, V. Beach Profiling and LIDAR Bathymetry: An Overview with Case Studies. *J. Coast. Res.* **2011**, *27*, 1019–1028. [CrossRef]
18. O'Dea, A.; Brodie, K.L.; Hartzell, P. Continuous Coastal Monitoring with an Automated Terrestrial Lidar Scanner. *J. Mar. Sci. Eng.* **2019**, *7*, 37. [CrossRef]
19. Caballero, I.; Stumpf, R.P. On the use of Sentinel-2 satellites and lidar surveys for the change detection of shallow bathyme-try: The case study of North Carolina inlets. *Coast. Eng.* **2021**, *169*, 103936. [CrossRef]
20. Thuan, D.H.; Almar, R.; Marchesiello, P.; Viet, N.T. Video Sensing of Nearshore Bathymetry Evolution with Error Estimate. *J. Mar. Sci. Eng.* **2019**, *7*, 233. [CrossRef]
21. Carlson, D.F.; Fürsterling, A.; Vesterled, L.; Skovby, M.; Pedersen, S.S.; Melvad, C.; Rysgaard, S. An affordable and portable autonomous surface vehicle with obstacle avoidance for coastal ocean monitoring. *HardwareX* **2019**, *6*, e00059. [CrossRef]
22. Archetti, R.; Damiani, L.; Bianchini, A.C.; Romagnoli, C.; Abbiati, M.; Addona, F.; Airoldi, L.; Cantelli, L.; Gaeta, M.G.; Guerrero, M.; et al. Innovative strategies, monitoring and analysis of the coastal erosion risk: The Stimare Project. In Proceedings of the 29th International Ocean and Polar Engineering Conference, ISOPE 2019, Honolulu, HI, USA, 16–21 June 2019; Volume 3, pp. 3836–3841.
23. Martinelli, L.; Zanuttigh, B.; De Nigris, N.; Preti, M. Sand bag barriers for coastal protection along the Emilia Romagna littoral, Northern Adriatic Sea, Italy. *Geotext. Geomembr.* **2011**, *29*, 370–380. [CrossRef]
24. Regione Emilia Romagna. *New Tools for Coastal Management in Emilia-Romagna*; Montanari, R., Marasmi, C., Eds.; Regione Emilia Romagna: Bologna, Italy, 2012; p. 61.

25. Idroser. Progetto di Piano per la Difesa dal Mare e la Riqualificazione Ambientale del Litorale della Regione Emilia-Romagna. In *AA.VV.*; Regione Emilia Romagna: Bologna, Italy, 1996; p. 365.

26. Arpa. Stato del Litorale Emiliano-Romagnolo all'anno 2000. In *I quaderni di Arpa*; Preti, M., Ed.; Arpa Emilia Romagna: Bologna, Italy, 2002; p. 224. ISBN 88-87854-10-6.

27. Arpa. Stato del Litorale Emiliano-Romagnolo all'anno 2007 e piano decennale di gestione. In *I Quaderni di Arpa*; Preti, M., De Nigris, N., Morelli, M., Monti, M., Bonsignore, F., Aguzzi, M., Eds.; Arpa Emilia Romagna: Bologna, Italy, 2009; p. 270. ISBN 88-87854-21-1.

28. Arpae. Stato del Litorale Emiliano-Romagnolo al 2012. Erosione e Interventi di Difesa. In *I Quaderni di Arpae*; Aguzzi, M., Bonsignore, F., De Nigris, N., Morelli, M., Paccagnella, T., Romagnoli, C., Unguendoli, S., Eds.; Arpa Emilia Romagna: Bologna, Italy, 2016; p. 227. ISBN 978-88-87854-41-1.

29. Vecchi, E.; Aguzzi, M.; Albertazzi, C.; De Nigris, N.; Gandolfi, S.; Morelli, M.; Tavasci, L. Third beach nourishment project with submarine sands along Emilia-Romagna coast: Geomatic methods and first monitoring results. *Rend. Lincei Sci. Fis. Nat.* **2020**, *31*, 79–88. [CrossRef]

30. Arpae. Monitoraggio morfologico e sedimentologico delle 8 spiagge oggetto di ripascimento—Monitoraggio morfologico dell'area al largo di prelievo delle sabbie—Rete Geodetica Costiera. In *Risultati, AA.VV.*; Arpae Emilia Romagna: Bologna, Italy, 2019; p. 249.

31. Lamberti, A.; Mancinelli, A. Italian experience on submerged barriers as beach defence structures. In Proceedings of the Coastal Engineering Proceedings, Orlando, FL, USA, 2–6 September 1996; Volume 1, pp. 2352–2365.

32. Poulain, P.M.; Kourafalou, V.H.; Cushman-Roisin, B. Northern Adriatic Sea. In *Physical Oceanography of the Adriatic Sea Past, Present and Future*; Cushman-Roisin, B., Gacic, M., Poulain, P.M., Artegiani, A., Eds.; Kluwer Academic Publishers: Dordrecht, The Netherlands, 2001. [CrossRef]

33. Lionello, P.; Cavaleri, L.; Nissen, K.M.; Pino, C.; Raicich, F.; Ulbrich, U. Severe marine storms in the Northern Adriatic: Characteristics and trends. *Phys. Chem. Earth Parts A/B/C* **2012**, *40–41*, 93–105. [CrossRef]

34. Arpae. Available online: http://www.smr.arpa.emr.it/dext3rhttps://www.arpae.it/sim/?mare/boa (accessed on 27 December 2020).

35. Masina, M.; Ciavola, P. Analisi dei livelli marini estremi e delle acque alte lungo il litorale ravennate. *Studi Costieri* **2011**, *18*, 87–101.

36. Fabbri, S.; Giambastiani, B.M.S.; Sistilli, F.; Scarelli, F.; Gabbianelli, G. Geomorphological analysis and classification of foredune ridges based on Terrestrial Laser Scanning (TLS) technology. *Geomorphology* **2017**, *295*, 436–451. [CrossRef]

37. Mancini, F.; Dubbini, M.; Gattelli, M.; Stecchi, F.; Fabbri, S.; Gabbianelli, G. Using Unmanned Aerial Vehicles (UAV) for High-Resolution Reconstruction of Topography: The Structure from Motion Approach on Coastal Environments. *Remote. Sens.* **2015**, *5*, 6880–6898. [CrossRef]

38. Scarelli, F.; Sistilli, F.; Fabbri, S.; Cantelli, L.; Barboza, E.; Gabbianelli, G. Seasonal dune and beach monitoring using photogrammetry from UAV surveys to apply in the ICZM on the Ravenna coast (Emilia-Romagna, Italy). *Remote. Sens. Appl. Soc. Environ.* **2017**, *7*, 27–39.

39. Perini, L.; Calabrese, L.; Deserti, M.; Valentini, A.; Ciavola, P.; Armaroli, C. Le mareggiate e gli impatti sulla costa in Emilia-Romagna 1946–2010. In *I quaderni di Arpa*; Arpa Emilia Romagna: Bologna, Italy, 2011.

40. Dolan, R.; Davis, R.E. An intensity scale for Atlantic coast northeast storms. *J. Coast. Res.* **1992**, *8*, 352–364.

41. Mendoza, E.; Jiménez, J. Storm-Induced Beach Erosion Potential on the Catalonian Coast. *J. Coast. Res.* **2004**, *48*, 81–88.

42. Archetti, R.; Paci, A.; Carniel, S.; Bonaldo, D. Optimal index related to the shoreline dynamics during a storm: The case of Jesolo beach. *Nat. Hazards Earth Syst. Sci.* **2016**, *16*, 1107–1122. [CrossRef]

43. Preti, M. I due interventi di ripascimento con sabbie sottomarine realizzati in Emilia-Romagna nel 2002 e nel 2007. *Studi Costieri* **2011**, *19*, 7–9.

44. Preti, M.; Aguzzi, M.; Costantino, R.; De Nigris, N.; Morelli, M. Monitoraggio delle spiagge nel periodo 2007–2009. *Studi Costieri* **2011**, *19*, 137–198.

45. Cavaleri, L.; Bajo, M.; Barbariol, F.; Bastianini, M.; Benetazzo, A.; Bertotti, L.; Chiggiato, J.; Ferrarin, C.; Umgiesser, G.; Trincardi, F. The 2019 Flooding of Venice and Its Implications for Future Predictions. *Oceanography* **2020**, *33*, 42–49. [CrossRef]